GEOPHYSICAL RESEARCH LETTERS, VOL. 28, NO. 17, PAGES 3341-3344, SEPTEMBER 1, 2001

215

Coseismic interferograms of two M_S = 6.6 earthquakes in the South Iceland Seismic Zone, June 2000

Rikke Pedersen[1], Freysteinn Sigmundsson[1], Kurt L. Feigl[2], and Thóra Árnadóttir[1]

[1]Nordic Volcanological Institute, Reykjavik, Iceland, [2]CNRS, Toulouse, France

Abstract. We present InSAR observations of deformation due to two M_S = 6.6 earthquakes in the South Iceland Seismic Zone in June 2000. Coseismic deformation predominates in the ERS interferograms. Range change, due to mainly right-lateral strike-slip on N-S striking faults, amounting to more than 15 cm is observed, although displacement is mainly perpendicular to the satellite look direction. Using elastic dislocation models in a trial-and-error scheme, we find a best-fitting model that agrees well with the aftershock locations and moment magnitudes estimated from seismograms. The June 17 model has a fault patch 16 km long, 10 km deep, striking N05°E, dipping 86°, with a slip maximum of 2.40 m. The June 21 model has a vertical patch 15 km long, 9 km deep, striking N01°W, with a slip maximum of 2.15 m.

Introduction

The mid-Atlantic plate boundary passes through South Iceland as a series of ridge segments connected by a transform zone, known as the South Iceland Seismic Zone (SISZ) (Fig. 1). There, an array of N-S striking surface fractures has been mapped [e.g., *Einarsson & Eiríksson*, 1982; *Einarsson & Sæmundsson*, 1992; *Einarsson*, unpublished data, 2001]. The fractures indicate a tectonic phenomenon described as book-shelf faulting [e.g., *Sigmundsson et al.*, 1995], i.e. right-lateral faulting on numerous parallel N-S striking planes, which accommodate an overall left-lateral E-W transform motion across the zone. Boundary element modeling, based on the mapped fractures, confirms the ability of N-S striking faults to take up the deformation in the area, if the faults are longer and more numerous than mapped [*Hackman et al.*, 1990].

Earthquakes in the SISZ tend to cluster in time. Historically, sequences of large, magnitude 6 or 7 earthquakes occur at intervals of 45 to 112 years [*Einarsson et al.*, 1981]. The last big earthquake, prior to 2000, occurred as a single M_S=7 event in 1912, at the eastern border of the SISZ. In the same area, an intermediate M_S = 5.8 event occurred in 1985. On the western side of the SISZ, magmatic activity in the Hengill volcanic system (Fig. 1) increased seismicity substantially between 1994 and 1998, culminating in two M_L = 5 earthquakes [*Feigl et al.*, 2000]. Estimated seismic moment release from 1700 through 1993 as a function of longitude reveal two distinct zones centered on 20.3°W and 20.7°W with relatively low strain release [*Stefánsson et al.*, 1993]. The June 2000 earthquakes [*Einarsson et al.*, 2000; *Stefánsson et al.*, 2000] occurred in both these zones.

Paper number 2001GL013235.
0094-8276/01/2001GL013235$05.00

The hypocenter of the June 17 earthquake was located at 63.975°N, 20.370°W at 6.3 km depth. Aftershocks indicate a fault 16 km long, striking N09°E and dipping 86° towards east, extending from the surface to a depth of 10 km [*Stefánsson et al.*, 2000]. The best double-couple fault plane solution from the *USGS* [2000] has a strike of N05°E, dip 83°, and rake 175°, with a seismic moment (M_0) estimate of 6.0×10^{18} N m and a moment magnitude (M_W) of 6.5 (M_W=((2/3)×log M_0)-6.03). The hypocenter of the June 21 event was located at 63.977°N, 20.713°W at 5.1 km depth. Aftershocks indicate a vertical 18 km long fault, striking N02°W, extending from the surface to 8 km depth [*Stefánsson et al.*, 2000]. The best double-couple fault plane solution from the *USGS* [2000] has a strike of N04°E, dip 84°, rake 172°, with a M_0 estimate of 5.2×10^{18} N m, giving M_W = 6.4.

Data and Methods

Interferometric analysis of Synthetic Aperture Radar (InSAR) images acquired by ERS1 and ERS2, has proven to be a valuable tool in studying crustal deformation [e.g., *Massonnet & Feigl*, 1998]. Precise modulated measurements of the distance ("range") change record ground movements during the time interval between two imaging epochs. Range change is measured along the line of sight (LOS) from ground to satellite. For the descending orbits used here, the LOS unit vector is [0.442, -0.117, 0.889] for track 52 at the epicenter of the June 17 event, and [0.387, -0.109, 0.916] for track 95 at the epicenter of the June 21 event in east, north, and upward components. Contours of range change appear as fringes, each representing a change of 28 mm for ERS data.

InSAR observations of deformation have been reported in several areas in Iceland [e.g., *Massonnet & Sigmundsson*, 2000; *Feigl et al.*, 2000]. Correlation of the radar images may be sufficiently high for interferometry only in the absence of snow cover, which severely limits the number of possible interferometric combinations covering Iceland. Most of our interferograms cover the southern part of the Eastern Volcanic Zone (EVZ) and the easternmost part of the SISZ, though one interferogram covers all of the SISZ (Fig. 1, Table 1). To calculate the interferograms, we used the PRISME/DIAPASON software developed by CNES, in the 2-pass approach described by *Massonnet & Feigl* [1998]. The digital elevation model, orbital modeling and filtering are equal to those used by *Feigl et al.* [2000].

Interferometric results

We have analyzed a series of 20 interferograms, composed of 11 SAR images, in ERS track 52, frame 2313, and one interferogram from ERS track 95, frame 2313 (Fig. 1). The

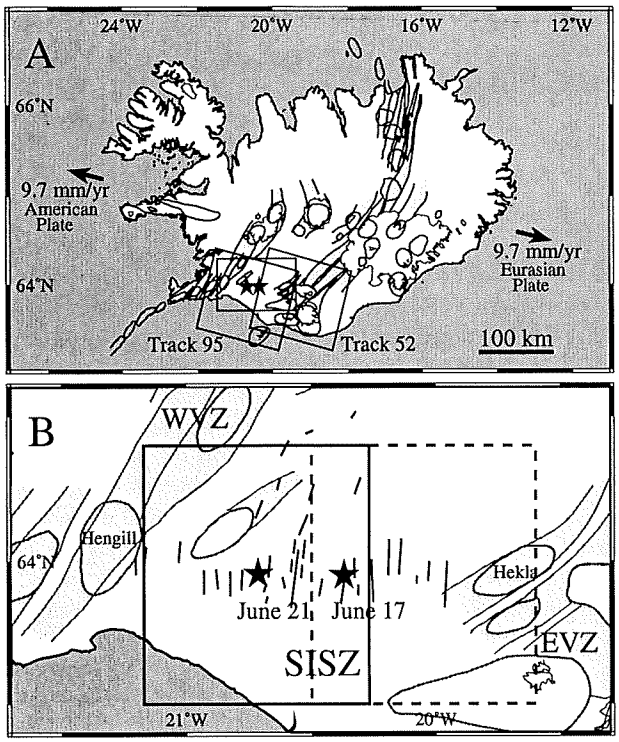

Figure 1: A) Volcanic systems of Iceland, icecaps, fissure-systems and fracture zones. After *Einarsson and Sæmundsson* [1992]. Stars mark epicenters. Large boxes delimit the ERS frames used; rectangular box the area shown in Fig. 1B.
B) The SISZ links the eastern (EVZ) and the western volcanic zone (WVZ). Boxes show outlines of the panels in Fig. 2.

images from track 52 span the time interval Aug. 3, 1993 to Sept. 29, 2000, to form pre-, co- and post-seismic image-pairs. Five of these image-pairs, and one additional pair from track 95, have been used in this study (Table 1).

The primary signal is strong coseismic deformation from the June 2000 earthquakes. Both caused predominantly right-lateral strike-slip movement on nearly vertical faults, striking roughly N-S. The ERS imaging geometry is completely insensitive to the displacement component parallel to the N11°E trend of the satellite trajectory. Consequently, the interferograms show mostly the vertical and east-west components of the displacement field. The fault trace of June 17 is located very close to the western margin of track 52. Therefore only deformation occurring east of the fault trace appears. The three coseismic interferograms from track 52 including the June 17 event also span June 21, but deformation due to the second event is limited in this track by the distance from the epicenter.

The preseismic interferogram (Fig. 2A) clearly shows that no significant deformation occurred in the area just east of the June 17 epicenter from Aug. 21, 1998 until June 16, 2000. The fringes seen at the eastern image margin are due to an eruption of the Hekla volcano Feb. 26 – March 8, 2000. The three coseismic interferograms shown in panels B, C and E of Fig. 2, all show consistent deformation pattern associated with the June 17 earthquake. The coseismic interferogram spanning 35 days (Fig. 2E) has very good coherence, and the deformation fringes to the north show up clearly. Range decreases in the southern lobe, and increases in the northern one. The straight blue fringe striking almost due east in Fig. 2E must correspond to a nodal plane for the June 17 focal mechanism. The absolute maximum range change cannot be determined due to incoherence in an area close to the surface rupture, but the fringes visible in the southern part of the image amount to approximately 15 cm of range decrease. In the vicinity of the fault trace local surface effects such as soil compaction, creation of local push-up structures, rotation of rocks due to shaking, and strain in excess of approximately 10^{-3}, can all cause loss of coherence. Our post-seismic interferogram (Fig. 2D) spans 35 days. It records no postseismic deformation in the area during September 2000.

The 35 day coseismic interferogram including the June 21 earthquake is shown in Fig. 2H, with a deformation pattern similar to the one created by the June 17 earthquake. Here the fringe pattern extends across the fault trace to the western side. The visible fringes in the southeastern lobe amount to roughly 18 cm of range decrease. Here also, coherence decays in the vicinity of the fault trace. However, the incoherent area is not as large as for the June 17 event. At the eastern margin of the image, we see deformation near the fault plane that ruptured on June 17.

Modeling of deformation

To explain the observed coseismic fringe pattern, we model finite rectangular dislocations buried in an elastic half-space [*Okada*, 1985]. We use the RNGCHN implementation [*Feigl & Dupré*, 1999], assuming a Poisson solid, a double-couple focal mechanism, and a LOS unit vector. The dislocation parameters were inferred using a trial-and-error fitting of the observed fringe patterns. We consider slip patches for both earthquakes with dimensions similar to the aftershock distribution (Fig. 2F and I). Uniform slip models were discarded, as trial-and-error tests showed that more slip is required near the centers of the faults. Initial parameters of a 3-patch model for the June 17 event were supplied by K. Ágústsson and A. Linde [personal communication, 2000], based on preliminary analysis of data from four volumetric strainmeters. We modified these parameters to produce a better fit to our data. The fringe pattern calculated from our best-fit model for the June 17 event appears in Fig. 2F. This model includes the effect due to the June 21 event, presented below. The inferred fault plane rupturing on June 17 has a dip of 86°, strikes N05°E, a length of 16 km and extends from the surface to 10 km depth (Table 2). The slip has a rake of 175°

Table 1. Interferometric pairs used in this study. All images acquired by the ERS-2 satellite (copyright by ESA). All pairs in track 52, frame 2313, except the final one, which is track 95, frame 2313. h_a is the altitude of ambiguity.

Fig	Orbit numbers	Master image	Slave image	Δtime (days)	h_a (m)
2A	17441-26960	Aug. 21, 1998	June 16, 2000	665	455.0
2B	11429-28463	July 27, 1997	Sept. 29, 2000	1190	-141.8
2C	11930-28463	Aug. 01, 1997	Sept. 29, 2000	1155	442.3
2D	27962-28463	Aug. 25, 2000	Sept. 29, 2000	35	62.6
2E	26960-27461	June 16, 2000	July 21, 2000	35	70.5
2H	27003-27504	June 19, 2000	July 24, 2000	35	-101.5

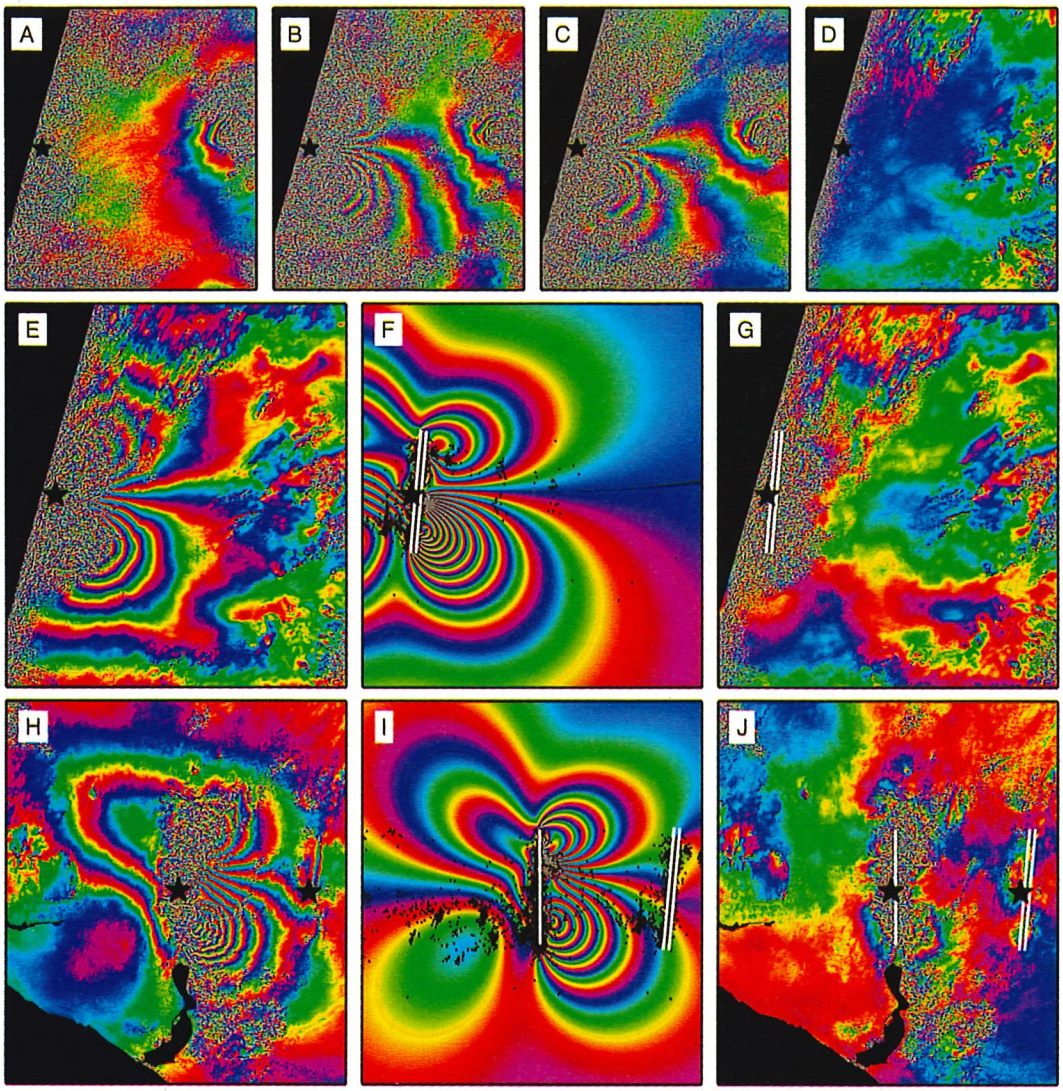

Figure 2: Observed, calculated and residual interferograms. One color fringe represents 28.3 mm of range change. All the images cover an area of 45 km east-west and 50 km north-south as outlined in Fig. 1. Black stars mark epicenters, and white lines mark the upper and lower boundary of the fault segments. Aftershocks shown as black dots. **Panels A through G:** Track 52, frame 2313: A: preseismic interval; B, C and E: coseismic intervals; D: postseismic interval; F: fringe pattern calculated from fault model; G: residual interferogram created by subtracting model (panel F) from observed interferogram (panel E). **Panel H through J:** Track 95, frame 2313: H: coseismic interval; I: fringe pattern calculated from fault model; J: residual interferogram created by subtracting model (panel I) from observation (panel H).

(slight thrusting) and is asym-metrically distributed with respect to the fault's center. On average 1.39 m of slip occurred south of the fault center, but 0.87 m north of it. Fig. 2G shows the residual interferogram.

The fringe pattern created from our best-fit model for the June 21 earthquake is shown in Fig. 2I. The modeled fault plane is vertical, strikes N01°W, has a length of 15 km and extends from the surface to 9 km depth. The slip is asymmetrically distributed with respect to the fault's center, but here most slip occurred to the north. On average 1.08 m of slip occurred south of the fault center, but 1.42 m north of it. The triggered or postseismic deformation near the fault trace created on June 17 was modeled by 10.5 cm of left-lateral slip, raking 20 degrees, on a 7 km long fault patch extending from 0.5 km below surface to 10 km depth, coinciding with a central part of the fault plane from June 17. Fig. 2J shows the residual interferogram; Table 2, all fault parameters.

Discussion and Conclusions

Our simple 7-patch model fits the InSAR observations quite well. The residual interferograms (Fig. 2G and 2J) show at most one unexplained fringe, equivalent to about 3 cm in range. Thus, coseismic slip explains more than 80% of the observed signal. Both the modeled fault slip patches have a strike similar to previously mapped faults in the SISZ. However, the modeled faults are longer, in good agreement with the boundary element modeling done by *Hackman et al.* [1990]. Our geodetic moment estimates are 5.44×10^{18} N m and 5.06×10^{18} N m for the June 17 and June 21 events, respectively, assuming a shear modulus of 30 GPa, giving M_W 6.5 and 6.4, in excellent agreement with the USGS estimates.

For the June 17 event, surface fractures only occur in the central part of the fault trace where slip exceeds one meter, in agreement with *King* [1986], whose studies show that the rupture does not necessarily reach the surface unless it

Table 2. Fault parameters for the best-fit models. Latitude and longitude given for the lower southern corners of the fault patches. Segments extend to the surface except the last one, showing inferred triggered slip terminating at 0.5 km depth.

June 2000	Lon (°)	Lat (°)	Length (km)	Width (km)	Strike (°)	Dip (°)	Rake (°)	Total slip (mm)	U1 (mm)	U2 (mm)
17	-20.3581	63.9077	16.0	10.0	5E	86	175	250	-249	22
17	-20.3485	63.9569	8.0	10.0	5E	86	175	900	-897	78
17	-20.3537	63.9300	5.5	10.0	5E	86	175	1250	-1245	109
21	-20.7008	63.9146	12.0	9.0	1W	90	180	450	-450	0
21	-20.7018	63.9415	9.0	9.0	1W	90	180	1050	-1050	0
21	-20.7039	63.9954	6.0	9.0	1W	90	180	650	-650	0
21 trig	-20.3468	63.9658	7.0	9.5	5E	86	20	106	100	35

exceeds 1 meter. The InSAR based models are not unique, because of a trade-off between several fault parameters, such as dip versus width, and slip versus depth. The geometry of the fault that ruptured on June 21 appears to be more complex than that of June 17. Our model does not account for the entire deformation signal, especially in the vicinity of the southern part of the inferred fault trace, as apparent in the residual interferogram (Fig. 2J). Although this may be due to a combination of increased coherence and better spatial coverage, the differences in surface rupture support a more complex model. For instance, a 2.3-meter-wide surface fissure was found at an approximately 500-meter-long ENE-trending fracture, where our model calls for 1.5 meters of N-S striking strike-slip [A. Clifton, personal communication, 2001]. A comparison with the aftershock distribution (from June 21 to Nov. 22, 2000) reveals a cluster of aftershocks, just to the south of maximum slip in our model (Fig. 2I), indicating that the main event did not relieve all stress on the fault plane. The intensity of aftershocks has a maximum at the southern tip of the modeled fault, which might indicate inhibited southward fault migration.

The inferred slip on the fault plane that ruptured on June 17, in the period June 19, 2000 to July 24, 2000, is mostly left-lateral strike-slip, whereas the June 17 earthquake produced right-lateral strike-slip. We suggest that this "postseismic back-slip" was triggered by the June 21 earthquake, which forced the block between the two fault traces towards south. The residual signal, amounting to one closed, elliptical fringe of subsidence just east of the modeled fault plane of June 17, is most likely due to compaction of soil in a wet area where extensive surface ruptures were mapped.

Further work includes joint interpretation of InSAR, GPS and volumetric strain data, which together will provide a detailed image of the deformation created by the June 2000 earthquakes, and help test our hypothesis that the June 17 quake triggered the June 21 event by stress transfer.

Acknowledgments. G. Guðmundsson, Icelandic Meterological Office, provided aftershock locations from the SIL database. Comments from two anonymous reviewers improved the paper. ERS SAR images were provided through ESA Envisat grant A03-22 and ERS grant A03-200. A special grant from the Icelandic government to study the 2000 earthquakes is acknowledged. The GMT public domain software was used to prepare figures.

References

Einarsson, P., S. Björnsson, G. Foulger, R. Stefánsson and Þ. Skaftadóttir, Seismicity pattern in the South Iceland seismic zone, In *Earthquake prediction – an international review*, D.W. Simpson and P.G. Richards (editors), *Maurice Ewing Series* 4, 141-151, Am. Geophys. Union, 1981.

Einarsson, P., and J. Eiríksson, Earthquake Fractures in the Districts Land and Rangárvellir in the South Iceland Seismic Zone, *Jökull*, *32*, 113-119, 1982.

Einarsson, P., and K. Sæmundsson, Earthquake epicenters 1982-1985 and volcanic systems in Iceland (map), in *I hlutarsins eðli: Festschrift for Thorbjorn Sigurgeirsson*, T. Sigfússon (editor), Menningarsjóður, Reykjavík, 1992.

Einarsson, P., A. Clifton, F. Sigmundsson, and R. Sigbjornsson, The South Iceland Earthquakes of June 2000: Tectonic Environment and Effects, in *AGU Fall Meeting*, A.F. Spilhaus (editor), pp. F890, Am. Geophys. Union, San Francisco, 2000.

Feigl, K.L., and E. Dupré, RNGCHN: a program to calculate displacement components from dislocations in an elastic half-space with applications for modeling geodetic measurements of crustal deformation, *Computers & Geosciences*, *25*, 695-704, 1999.

Feigl, K.L., J. Gasperi, F. Sigmundsson, and A. Rigo, Crustal deformation near Hengill volcano, Iceland 1993-1998: Coupling between magmatic activity and faulting inferred from elastic modeling of satellite radar interferograms, *J. Geophys. Res.*, *105*, 25,655-25,670, 2000.

Hackman, M.C., G.C.P. King, and R. Bilham, The Mechanics of the South Iceland Seismic Zone, *J. Geophys. Res.*, *95*, 17339-17351, 1990.

King, G.C.P., Speculations on the Geometry of the Initiation and Termination Processes of Earthquake Rupture and its Relation to Morphology and Geological Structure, *Pure App. Geophys.*, *124*, 567-585, 1986.

Massonnet, D., and K.L. Feigl, Radar Interferometry and its application to changes in the Earth's surface, *Rev. Geophys.*, *36*, 441-500, 1998.

Massonnet, D., and F. Sigmundsson, Remote Sensing of Volcano Deformation by Radar Interferometry from Various Satellites, in *Remote Sensing of Active Volcanism*, P.J. Mouginis-Mark, J.A. Crisp and J.H. Fink (editors), pp. 207-221, AGU, 2000.

Okada, Y., Surface deformation to shear and tensile faults in a half-space, *Bull. Seism. Soc. Am.*, *75*, 1135-1154, 1985

Sigmundsson, F., P. Einarsson, R. Bilham, and E. Sturkell, Rift-transform kinematics in south Iceland: Deformation from Global Positioning System measurements, 1986 to 1992, *J. Geophys. Res.*, *100*, 6235-6248, 1995.

Stefánsson, R., R. Böðvarsson, R. Slunga, P. Einarsson, S. Jakobsdóttir, H. Bungum, S. Gregersen, J. Havskov, J. Hjelme, and H. Korhonen, Earthquake prediction research in the south Iceland seismic zone and the SIL project, *Bull. Seims. Soc. Am.*, 83, 696-716, 1993.

Stefánsson, R., G.B. Guðmundsson, and P. Halldórsson, The two large earthquakes in the South Iceland seismic zone on June 17 and 21, 2000, http://hraun.vedur.is/ja/skyrslur/June17and21_2000/index.html, 2000.

USGS, Nat'l Earthquake Info. Center: Previous Fast Moments, http://wwwneic.cr.usgs.gov/neis/FM/previous/0006.html, 2000

R. Pedersen, F. Sigmundsson and Th. Árnadottir, Nordic Volcanological Institute, Grensásvegur 50, 107 Reykjavik, Iceland. (rikke@norvol.hi.is, fs@norvol.hi.is, thora@norvol.hi.is)

K. L. Feigl, Centre National de la Recherche Scientifique, 14 Avenue E. Belin, 31400 Toulouse, France. (Kurt.Feigl@cnes.fr)

(Received March 28, 2001; revised June 14, 2001; accepted June 28, 2001.)